Aerial wetting contact angle measurement using confocal microscopy

Jacob W. Chesna[1,2], Bob F. Wiedmaier[2], Jinlin Wang[2], Ayman Samara[3], Richard K. Leach[4], Tsing-Hua Her[5], Stuart T. Smith[6]

[1]International Precision Engineering, Inc., Miami FL 33132, USA.

[2]Intel Corporation, Chandler AZ 85226, USA.

[3]Qatar Environment and Energy Research Institution, Hamad Bin Khalifa University-Qatar Foundation, Education City, Doha, Qatar

[4]Manufacturing Metrology Team, Faculty of Engineering, University of Nottingham NG7 2RD, UK

[5]Department of Physics and Optical Science, UNC Charlotte, Charlotte NC 28223, USA.

[6]Center for Precision Metrology, UNC Charlotte, Charlotte NC 28223, USA.

Abstract

A method is presented in which the wetting contact angle of a sessile drop is acquired aerially using confocal techniques to measure the radius and the height of a droplet deposited on a planar surface. The repeatability of this method is typically less than 0.25°, and often less than 0.1°, for droplet diameters less than 1 mm. To evaluate accuracy of this method, an instrument uncertainty budget is developed, which predicts a combined uncertainty of 0.91° for a 1 mm diameter water droplet with a contact angle of 110°. For droplets having diameters less than 1 mm and contact angles between 15° and 160°, these droplets approach spherical shape and their contact angles can be computed analytically with less than 1 % error. For larger droplets, gravitational deformation needs to be considered.

1. Introduction

The sessile drop method is a measurement technique that is used to investigate interfacial systems [1-4]. The key concept of sessile drop method is to evaluate the angle of intersection made by the liquid surface of a sessile drop and the substrate on which the drop rests. The angle of intersection is more

commonly known as the wetting contact angle and, in a simplistic sense, is a relative measure of the ratio between the cohesion forces within the liquid bulk and the adhesion forces between the liquid and the substrate. While the mechanics of droplet deposition and geometric measurement involve the control and influence of many interdependent experimental conditions, the interpretation of contact angles is well documented and, therefore, not discussed herein [see 5-8 for background].

Sessile drops have historically been measured using contact angle goniometers. A contact angle goniometer is comprised of a stage where the substrate, including the sessile drop is placed, and a camera. To optically measure the wetting contact angle, the camera is positioned so that its focal plane is approximately perpendicular to the substrate plane and coincident with the axis of symmetry on the drop. For illustration, an image used to determine the wetting contact angle of a 2.5 μl glycerin drop on a silica substrate using the sessile drop method with a goniometer is shown in Figure 1.

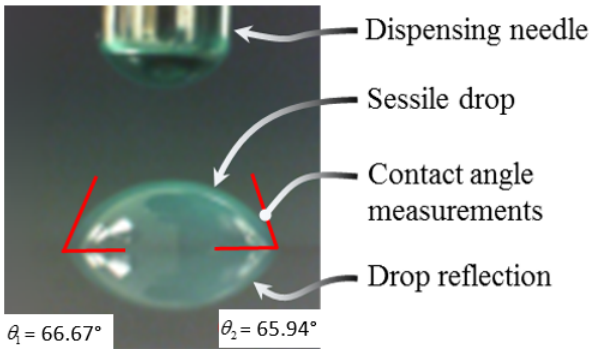

Figure 1: Wetting contact angle measurement of a 2.5 μl water sessile drop resting on a silica substrate using the sessile drop method with a contact angle goniometer.

From Figure 1, the limitations of contact angle goniometry are apparent. First, and most importantly, contact angle goniometry requires a clear line of sight to the triple phase contact line (i.e. the locus of points where solid, liquid and air are coincident). Second, edge detection is difficult because the boundary between blocked and unblocked light is defined by a highly reflective and tangential surface. Finally, if the camera angle is too low to view the reflection, or the contact angle approaches 90°, the location of the triple phase contact line on the substrate becomes difficult to distinguish. Another significant limitation arises with in-situ testing of a component where the line of sight to the droplet may be obscured, either by

features on the component itself, or by other components in an assembly. One example of a challenging application occurs in the semiconductor manufacturing industry, where flip-chip dies are mounted on organic substrates such that the die bumps made with arrays of solder bumps. This packaging technique includes the deposition of epoxy underfill near the edge of the die, which is then drawn beneath the die into the interstitial spaces between connections by capillary action, which is driven by the surface energy of the surfaces and the surface tension of the underfill. Measuring how well the substrate solder resist surface wets is critical to the development of materials and assembly processes. One challenge, however, is that in situ testing is difficult as it is typical to have other components, such as capacitors and dies, mounted to the substrate that restrict the clear line of sight. In addition, the traditional sessile drop method requires a drop size on the order of a microlitre, which necessitates the droplet to be placed far away from the solder bump field. What is the needed is a method that can use much smaller droplets to be placed as close to the bump field as possible, and does not depend upon a clear line of sight horizontally across the substrate.

To overcome the limitations outlined above, an aerial contact angle measurement method has been developed [8]. This technique uses a scanning confocal microscope to image the sessile drop from above and uses a geometric model to calculate the wetting contact angle.

2. Measurement principle

For small sessile drops, it is plausible to assume that the liquid/air interface is spherical in form, which is referred to as the spherical approximation herein. Additionally, in most metrological applications it can be assumed that the substrate is planar and that the optical axis of the imaging system is aligned perpendicularly to the substrate. With these assumptions, the contact angle θ_c of a sessile drop can be calculated from the measured droplet radius r_m and the height h_m relative to the substrate using

$$\theta_c = \cos^{-1}\left(1 - \frac{h_m}{r_m}\right). \tag{1.1}$$

In this work we measure the radius and the height of the droplets using a laser scanning confocal microscope [9,10]. The conventional output from an Olympus LEXT laser scanning confocal microscope (Model OLS 4000) is shown in Figure 2, along with illustrations of the radius (via a least-squares fit to a sphere) and the height (distance from apex of the fitted sphere to a planar fit of the substrate) of the droplet. More specifically, this microscope outputs a two dimensional matrix of surface heights, herein referred to as a surface map. Using this surface map and algorithms that fit the sphere and plane, the calculation of the wetting contact angle then becomes straightforward using equation (1.1).

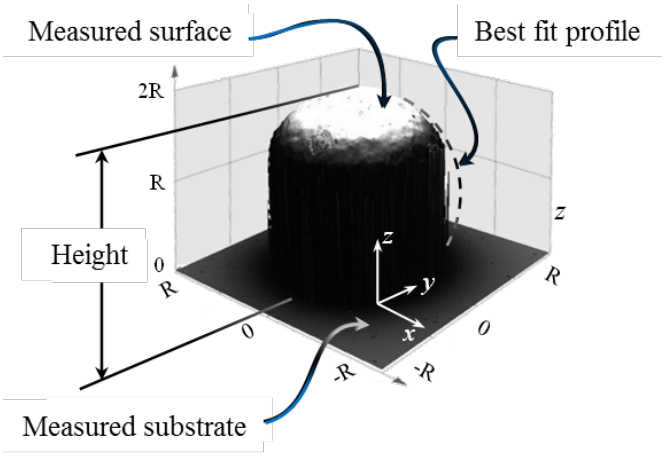

Figure 2: Confocal image of an 80 μm diameter gold sphere resting on a silica substrate using the conventional output of laser scanning confocal microscope.

In practice, only an upper portion of the surface map is accurate because of the slope limitations of the technique. There are two reasons for this slope limitation. The first is the loss of signal from specular surfaces with increasing slope. As a result of this, the measurement uncertainty associated with fitting a sphere to a partial dataset increases non-linearly as the measurement area (or the included angle of the measured patch) is reduced [11]. Secondly, there are additional slope dependent errors in the surface map inherent to the transfer function of the instrument [12-14]. As an example, a perfect sphere will be measured as a paraboloid with its original at the apex. This will produce an additional term to the uncertainty budget.

When the surface map proves to be inaccurate, the measurement of wetting contact angle can be improved by using an advanced confocal technique to measure the radius directly. The basic principle

behind the advanced confocal technique uses the difference in the relative locations of the cats-eye condition (when the focal point is coincident with the apex of surface) and the confocal condition (when the focal point is coincident with the centre of curvature) as a measure of the radius of curvature [15-18]. A schema is shown in Figure 3. A complete theoretical discussion of the optical response for a scanning confocal microscope, when measuring small spheres, is outlined elsewhere [18, 19].

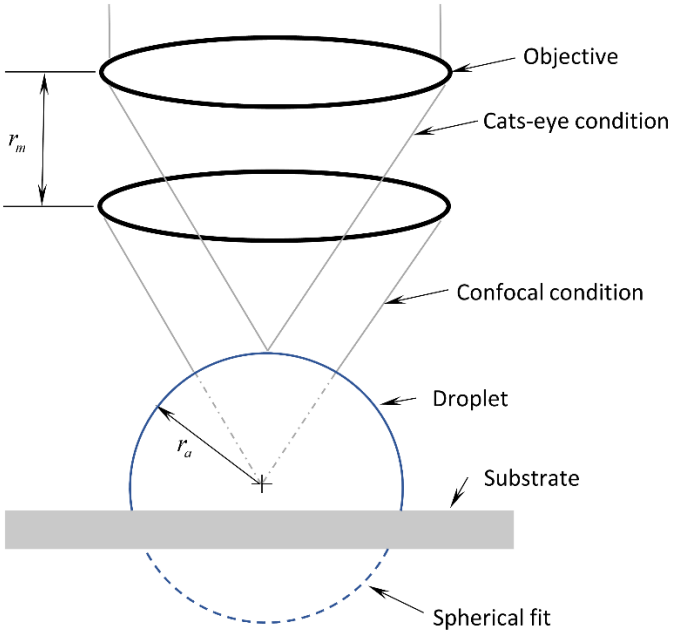

Figure 3: Conditions where radius measurement is possible when using a converging wavefront optical instrument.

2.1 Radial measurement using commercial confocal instruments

Typically commercial confocal microscopes provide only two forms of data output; a planar preview (horizontal slice) and the surface map. An illustration of slice orientation is shown as Figure 4. To provide data for subsequent analysis, code was implemented on a Keyence Violet Color 3D laser scanning microscope (Model VK-9701K) that automated the collection of the vertical confocal planes for analysis. Also, the surface topography information embedded in the measurement file of the Olympus LEXT was extracted with both data sets being analyzed using MATLAB.

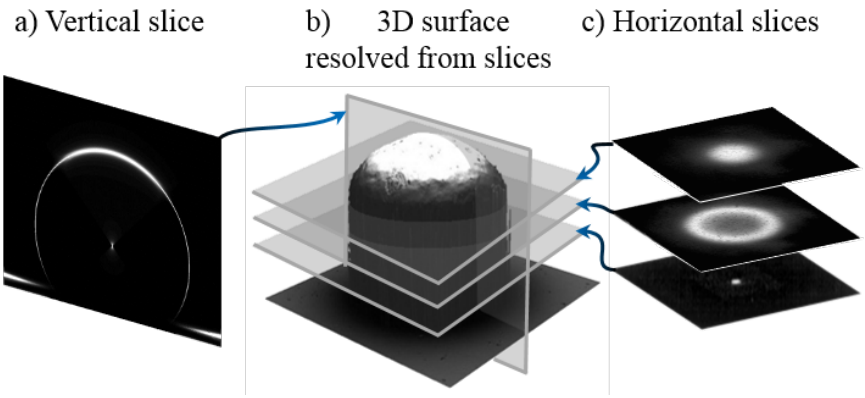

Figure 4: Schema of scanning plane orientation in a scanning confocal microscope with a vertical slice shown at left, a 3D image at centre with horizontal and vertical slices indicated, and a set of three horizontal confocal image slices on the right.

To be able to use the cat's eye/confocal measurement technique, a vertical confocal slice, including the axis of symmetry of the sessile drop, must be obtained. For reference, let a confocal slice be defined as a 2D image selectively extracted from the irradiance values for each voxel from a 3D scan, or the irradiance values from each pixel along the path of a 2D scan. If the location of the axis of symmetry relative to the scan boundaries is unknown, then the extraction of the vertical confocal slice may require the analysis of the irradiance data from the entire 3D scan volume (typically file sizes exceed one gigabyte). To increase measurement efficiency, the location of the axis of symmetry, and general shape of the drop, can be obtained using a coarse resolution scan, and then the regions of interest can be re-scanned with a higher resolution. These regions include the area around the substrate, the centre of curvature (confocal position) and the drop apex (cats-eye position). Another procedure to increase the quality of measurement is to adjust the illumination intensity for each area of interest to maximise signal to noise ratios. This is possible because changes in illumination between each area of interest will not impact the measured location of the features. An example of a vertical slice indicating the location of significant measurement features is shown in Figure 5.

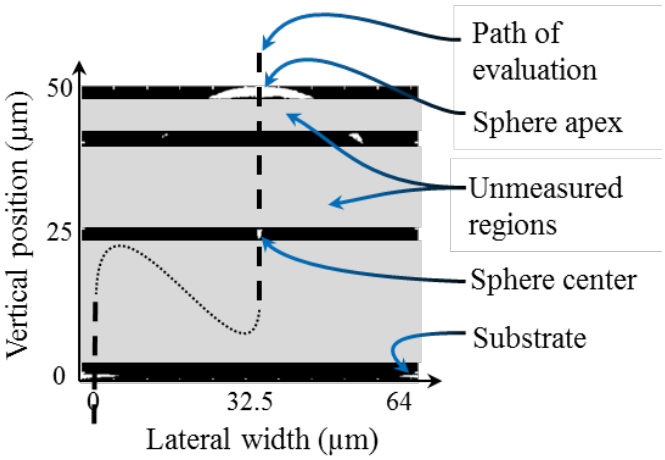

Figure 5: Vertical confocal slice, contrast enhanced, showing the resulting measurement of a 50 μm diameter silica sphere resting on a silica substrate. Also shown is the line (labeled "Path of evaluation") along which the irradiance was used for feature measurement. Note: grey regions were not recorded to expedite measurement time.

With the confocal slice acquired, the irradiance values along a path of evaluation can be analysed for the computation of the location of the features, see Figure 5. An example showing the irradiance, or more generally the intensity, as a function of distance along the path of evaluation is shown in Figure 6.

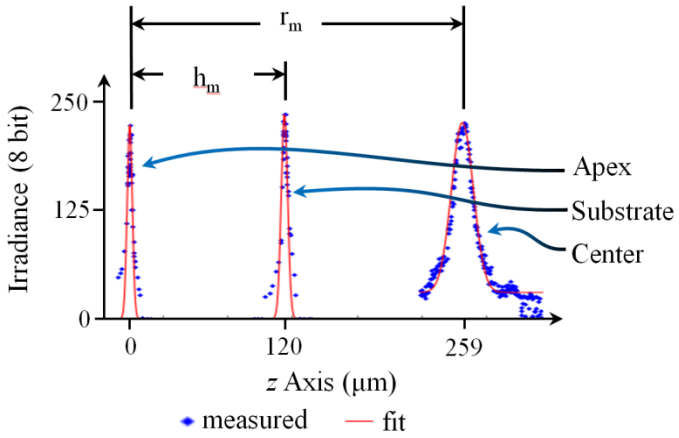

Figure 6: Plot of irradiance against z location along the path of evaluation of a 500 μm diameter stainless steel sphere set in a gauge block to exhibit an apparent contact of 57°. The diamonds represent the measured data points and the line represents a least-squares Gaussian fit.

Once the irradiance values along the path of evaluation have been extracted, the relative location of each feature can be obtained using least-squares fitting to a Gaussian function [23]. Because the instrument response of the Keyence scanning confocal microscope was repeatedly symmetric, the maximum of a Gaussian fit was used to identify the location of the features. Note that, depending on the

contact angle being above or below 90°, the center of the spherical fit could be higher than or below the measured location of the substrate (see Fig. 3). After the relative locations have been identified, equation (1.1) can be used to calculate the wetting contact angle.

3 Experimental Results

3.1 Measurements on sessile drops

The wetting contact angle of a set of 5 μl glycerin drops resting on a silica substrate was measured using both the Keyence confocal microscope and an AST Products Video Goniometric Contact Angle System (Model 2540XE). Each measurement result shown in Table 1 is the result of a mean taken over five measurement trials.

Table 1: Comparison of contact angle measurement using the proposed confocal method vs. a traditional goniometry.

Artifact/Machine	**Confocal**	**Goniometer**	**Difference**
Drop #1	60.14 ˚	61.8˚	1.7 ˚
Drop #2	57.38˚	60.5˚	3.1˚
Drop #3	59.14˚	59.6˚	0.5˚

The measurements using the two techniques were taken within three hours of each other. In accordance with the sessile drop method, the time between drop deposition and wetting contact angle measurement should be minimised due to mechanical instabilities inherent in wetting systems (these include evaporation, long-term settling, etc.). To account for this time delay, the drop material was chosen to be glycerin (near zero evaporation rate) and the drops were deposited the day previous to measurement, after which the drop settles and is considered to be stable.

3.2 Comparison between measurement techniques

Three measurement types were employed for a baseline comparison between techniques, including goniometry, confocal and contact (described below). To enable the comparison with contact measurement, and to significantly improve the temporal stability of the specimens to be measured, a set of representative measurement artifacts were used. These artifacts (International Precision Engineering

Artifact Set Model 55SS-2013) consist of three gauge blocks (numbers 1, 2 and 3) each with a single row of five stainless steel spheres with diameters of 0.5 mm, 1 mm and 1.5 mm respectively, set into conical recesses to provide apparent contact angles of 55°±15°, 90 ±5°, and 110°±5° respectively. A similar artifact from the set is shown in Figure 7 and comprises a 5 by 5 array of 0.5 mm diameter spheres at a pitch of 0.8 mm.

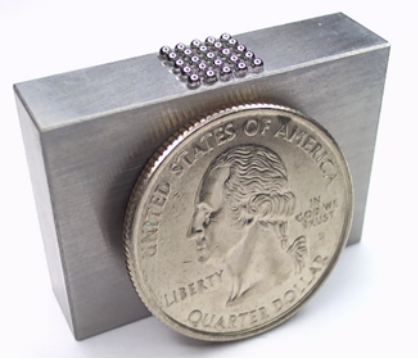

Figure 7: An image showing a 5 by 5 array of 0.5 mm diameter stainless steel spheres set into a gauge block surface to represent an array of temporally stable sessile drops. Also shown is a US quarter dollar coin for scale.

In addition to the two instruments mentioned in section 3.1, a Mitutoyo dial gauge (Model – ID-C112CEB 12.7-0.001 mm) referencing from a Mitutoyo precision granite stand (Model 527-896 Grade A) was used to measure the height of the spheres relative to the gauge block surface. All three measurement sets were conducted in temperature controlled environments, and all (except one) using equation (1.1) to calculate the measured contact angle. The exception was the case of contact measurement, where the measured radius, r_m , was taken as half the measured diameter of the spheres.

The results from the three techniques are shown in Table 2. For reference, the nominal results shown are calculated from an average of five measurement trials. An estimated measurement uncertainty is provided and was calculated as either: the standard deviation across the five measurements in the goniometer measurements; as the minimum contact angle that can be theoretically resolved using the least count of the dial gauge (1 μm) in the case of the contact measurements; from the procedures outlined in section 4 for the confocal measurements.

Table 2: Comparison of the proposed confocal, traditional goniometric, and direct contact methods. Measurements are carried out on a set of artifacts that were designed to simulate sessile drops.

Artifact/Setting	Confocal	Goniometer	Contact	Maximum deviation
∅0.5 mm #1a	45.34° ± 0.22°	42.8° ± 2.3°	44.80° ± 0.36°	2.5°
∅0.5 mm #1b	57.46° ± 0.22°	54.0° ± 7.6°	56.86° ± 0.35°	3.5°
∅0.5 mm #1c	61.69° ± 0.22°	60.5° ± 7.5°	61.10° ± 0.33°	1.2°
∅1.0 mm #2a	90.68° ± 0.12°	93.9° ± 4.9°	91.07° ± 0.16°	3.2°
∅1.0 mm #2b	85.39° ± 0.12°	92.9° ± 6.5°	85.01° ± 0.16°	7.9°
∅1.0 mm #2c	90.68° ± 0.12°	92.5° ± 4.0°	90.07° ± 0.16°	2.5°
∅1.5 mm #3a	107.00° ± 0.10°	107.5° ± 3.2°	106.28° ± 0.13°	1.2°
∅1.5 mm #3b	112.52° ± 0.10°	115.8° ± 2.0°	111.65° ± 0.13°	4.1°
∅1.5 mm #3c	113.50° ± 0.10°	116.5° ± 1.7°	112.90° ± 0.13°	3.6°

The maximum deviation between all measurements was 7.9°. This comparison should be reviewed with the note that the scales of the artifacts are smaller than that for which the AST goniometer was designed to measure. However, this was used because it is the only commercial instrument capable of measuring these parameters. If only the confocal and contact measurement techniques are compared (those with the highest degree of confidence in measurement), the maximum deviation is 0.87° when measuring the 1.5 mm #3b artifact.

For the purposes of estimating a combined measurement uncertainty, when using the Keyence confocal microscope to measure sessile drops, the standard deviation of the measured differences between the confocal microscope and the contact measurement technique is used as a measure of instrument bias. This instrument bias, u_b, was calculated to be 0.36° in this case.

3.3 Repeatability of radial measurement using surface map

To determine the contribution of radius uncertainty, u_{rm}, to the combined measurement uncertainty, a single sphere of the Number 1 International Precision Engineering gauge block was repeatedly measured using the Olympus confocal microscope. For reference, the microscope was configured with a

20× objective having a numerical aperture (NA) of 0.6. A best fit radius was determined using a four degree of freedom least-squares algorithm (radius and the Cartesian location of the centre of curvature) and the surface map of each measurement. To ensure consistent results, the surface map was filtered using a circular mask with a radius of 160 μm, determined by an acceptance angle of 40°, which is typical for 0.6 NA. The best fit radii and each corresponding standard deviation are shown in Table 3. For reference, each data set encompassed approximately 200,000 data points, and the average measured radii was found to be 255.6 μm, with a standard deviation of 1.98 μm across the seven measurements.

Table 3: Best fit radii from repeated measurements on a single sphere.

Trial	**Best fit radius/μm**	**Standard deviation/μm**
1	254.20	1.46
2	254.00	1.93
3	253.82	1.43
4	256.55	1.49
5	255.48	1.48
6	259.48	1.57
7	255.60	1.54

3.4 Measurement of translucent objects

To validate this technique for translucent droplets, a 50 μm diameter silica sphere resting on a silica substrate (standard laboratory microscope slide) was measured using the Olympus confocal microscope. The microscope was configured to return irradiance readings at a vertical scan interval of 100 nm. The measured irradiance is plotted against height in Figure 8.

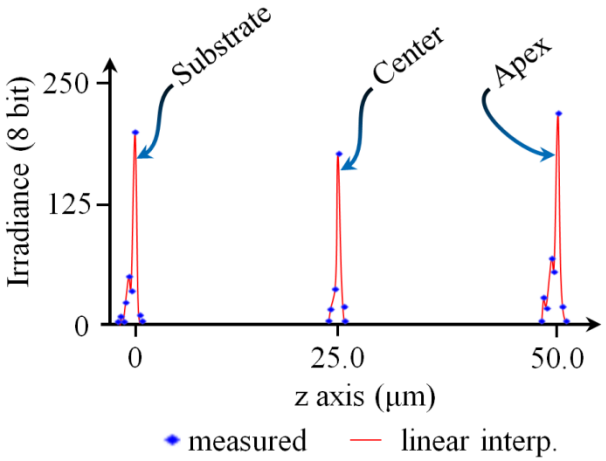

Figure 8: Plot of irradiance against z location along the path of evaluation (see Figure 5) of a 50 μm diameter silica sphere resting on a silica substrate.

The measured height, h_m, determined from the single peak values was found to be 50 μm and the measured radius, r_m, was 25 μm. This result, that the measured radius was equal to half the measured diameter, indicates consistency at 0.1 μm. The results of this experiment demonstrate the plausibility of using a confocal microscope to measure wetting contact angle on translucent objects resting on translucent surfaces. To improve the confidence of height and radii measurements on translucent spheres, it will be necessary to obtain spheres with substantially lower geometric uncertainties. To our knowledge, such spheres do not currently exist.

A more theoretically based evaluation of sphere measurement using confocal microscopes, along with the associated influences of interference, is outlined in reference [18]. With the support of both the measurements reported here and the theory outlined in [18], it is concluded that the interference caused by the recombination of light, at the scales investigated here, has a negligible impact on the calculated location of the features of interest in this work. As drop sizes approach the micrometre regime, the impact on feature location measurements on translucent objects must be revisited as it is clear that measurement anomalies exist from the recombination of light [18].

4 Uncertainty Analysis

At the time of writing, ISO specification standards to link the measured output of scanning confocal microscopes to a traceable measurement standard are still at draft stage [12], although some good practice guidance is available [13]. Such a specification standard would necessarily address slope dependent measurement errors [14] and a standardised approach to evaluate, and possibly compensate for, the optical transfer function [20]. Currently there are ongoing efforts to develop characterisation techniques for the use of an instruments optical transfer function in traceable measurements [21,22].

4.1 Instrument bias estimate

One source of error in dimensional measurements is due to instrument bias, u_b , which is difficult to determine. For our purposes we are comparing measurements of the steel sphere artifacts with contact measurements that are established and accepted to have low uncertainties. To gain a sense of the magnitude of this bias, the results in section 3.3 are compared with section 3.2. For reference, using contact method the diameter was 509.6 μm with a standard deviation of 0.63 μm over fourteen measurements (assumed radius of 254.8 μm). Using the confocal method the radius was 255.6 μm with a standard deviation of 1.98 μm across seven measurements. This difference of 0.8 μm is taken as an instrument bias.

4.2 Confocal characterisation

To measure the response characteristics of the Keyence confocal microscope, a single setting, 0.5 mm diameter #1b, in the stainless steel artifact set was measured repeatedly. The microscope was configured to use a 20× objective having an NA of 0.46. To characterise the instrument response to each feature, a high resolution scan was acquired. More specifically, the fine scan consisted of 350 confocal planes, 254 through the centre peak, 50 through the substrate surface, and 50 through the apex of the sphere, and with a minimum axial spacing between planes of 300 nm. As previously discussed, the laser intensity was adjusted between the scan of each feature (rather than each measurement) such that the maximum measured intensity of each feature was just below the detector saturation. The results of the

scan are shown in Figure 6 as a plot of the intensity values along the measurement path. It can be noted that the sampling spacing was not evenly distributed; rather there is a concentration of measured points around the regions of highest intensity and the regions with the highest changes in intensity per change in position. As shown in Figure 6, the apex, substrate and centre are clearly visible. Further, the detection of each feature, including the centre peak, are all indicative of a typical confocal microscope response which represents the instrument's point spread function at a singular measurement feature [23]. The Gaussian fit used a least-squares technique with four degrees of freedom, including amplitude, lateral and vertical offsets, and width. To decrease processing times, the amplitude was set as the maximum measured intensity value on each feature; the vertical offset was set to a value equal to the mean of the measurement noise. Additionally, to avoid measurement anomalies, each feature was measured using a filter to offset noise. More specifically, in these measurements the intensity data in each plane was averaged over a 5 by 5 pixel area.

The steel sphere artifact was measured seven times. After analysing the confocal data, the mean radius of the sphere was measured to be 257.61 μm with a standard deviation of 0.67 μm, and the mean height was measured to be 199.07 μm with a standard deviation of 0.76 μm. In practice, the uncertainty of measurement will include errors of the instrument itself, operator error and random variations in contact locations and forces (associated with operator errors). Because estimates for the first two sources are not known, both standard deviation values were then taken as the uncertainty in feature identification; where the uncertainty in measured radius, u_{rm}, is defined as the standard deviation in repeated radius measurements, and where the uncertainty in measured height, u_{hm}, is defined as the standard deviation in repeated height measurement.

4.3 Validity of spherical approximation

The measurement technique discussed here is largely based on the assumption that the drop is spherical. In practice, the profile of a sessile drop in the presence of a gravity field is governed by [7]:

$$\frac{dr}{d\varphi} = \frac{\gamma r \cos\varphi}{\rho g r z + \frac{2\gamma}{R} r - \gamma \sin\varphi}$$
$$\frac{dz}{d\varphi} = \frac{\gamma r \sin\varphi}{\rho g r z + \frac{2\gamma}{R} r - \gamma \sin\varphi} \quad (1.2)$$

where r and z are the lateral and vertical coordinates in a cylindrical coordinate system, φ is the slope at the point of interest, γ is the surface tension of the fluid at the air interface, ρ is the density of the liquid, g is the acceleration due to gravity, and R is the radius at the apex of the drop (see Figure 9 for illustrations of these parameters).

To assess the magnitude of the difference in contact angle due to hydrostatic deflection, a MATLAB programme was used to generate a matrix of differences; one for each radius, in the range from 1 μm to 1 mm, and for each contact angle in the range from 15˚ to 165˚. An illustration of the programme set up is shown as Figure 9. The programme generated a theoretical profile for each radius in the matrix (labeled Theoretical profile), and then, for every theoretical contact angle, an artificial horizon was established coincident to the point on the theoretical profile where the slope was equal to the theoretical contact angle (θ_t). Using the horizon as a boundary condition, a circular profile was fitted using a least-squares technique, from which the slope of the circle at the intersection of the horizon is determined (θ_f). The slope found on the best-fit circle at the intersection of the horizon was compared to the theoretical contact angle as a difference, Δ_θ. The resulting matrix of differences using water under standard gravity conditions is shown in Figure 10.

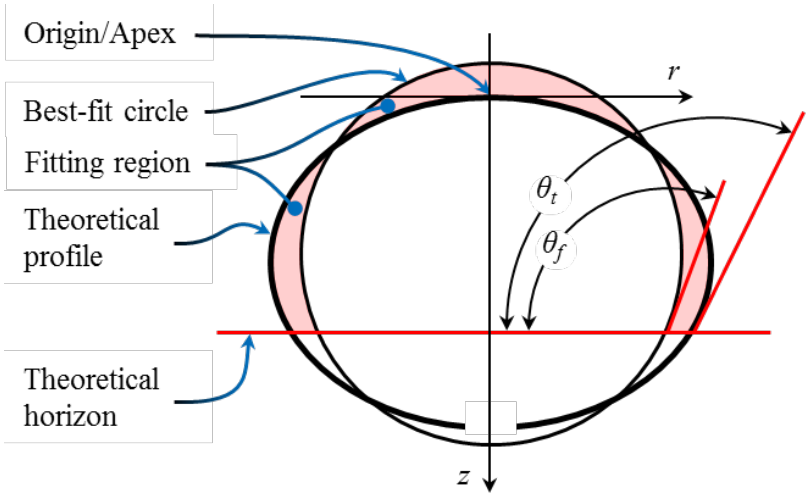

Figure 9: Schematic of best fit algorithm definitions.

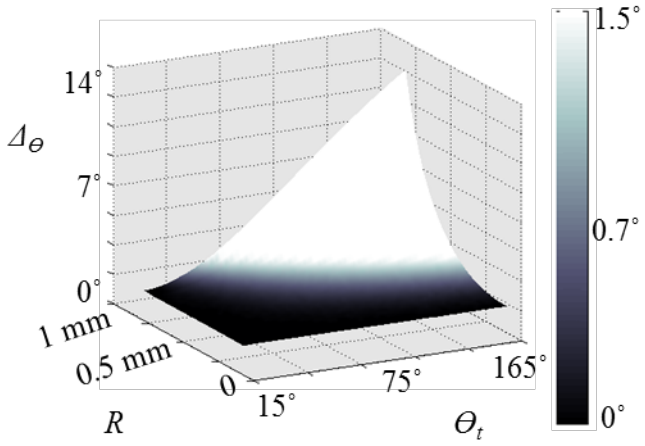

Figure 10: Plot of difference in contact angle of a water drop calculated from fitting a sphere to a theoretical axisymmetric profile of various water drops under the influence of gravity.

For simplicity, a bi-cubic surface was fitted to the matrix of differences as a simple means of estimating the uncertainty due to the spherical approximation, u_f. The equation for the bi-cubic surface is

$$u_f \approx \Delta_\theta \approx c_9 R^3 + c_8 \theta^3 + c_7 R^2 + c_6 R^2 \theta + c_5 R \theta^2 + c_4 \theta^2 + c_3 R + c_2 R \theta + c_1 \theta + c_0, \quad (1.3)$$

where the coefficients of the bi-cubic are tabulated in Tables 4, 5 and 6, each corresponding to an analysis using parameters for water, glycerin and mercury respectively and with units of radius, R, in metres, and

the units of the contact angle, θ, in radians. Note that the calculated standard deviation of the difference in the resulting matrix from analysis on a water droplet and the bi-cubic fit was calculated to be 0.21˚ using a matrix of 1350 differences. Calculations for mercury and glycerin droplets exhibited similar quality of fit.

Table 4: Coefficients for bi-cubic fit of difference in contact angles for a water drop due to a best fit sphere to a theoretical drop profile.

Coefficient	Value	Coefficient	Value
c_0	-0.0295	c_5	55.1550
c_1	0.0862	c_6	4.4035×10^4
c_2	-132.5997	c_7	1.9630×10^4
c_3	43.7745	c_8	0.0122
c_4	-0.0613	c_9	-3.3194×10^7

Table 5: Coefficients for bi-cubic fit of difference in contact angles for a glycerin drop due to a best fit sphere to a theoretical drop profile.

Coefficient	Value	Coefficient	Value
c_0	-0.0296	c_5	63.9552
c_1	0.0915	c_6	4.4702×10^4
c_2	-140.2542	c_7	4.9845×10^4
c_3	31.8736	c_8	0.0136
c_4	-0.0671	c_9	-5.1602×10^7

Table 6: Coefficients for bi-cubic fit of difference in contact angles for a mercury drop due to a best fit sphere to a theoretical drop profile.

Coefficient	Value	Coefficient	Value
c_0	-0.0269	c_5	71.5363
c_1	0.0916	c_6	4.0159×10^4
c_2	-136.8555	c_7	8.7851×10^4
c_3	10.6077	c_8	0.0146
c_4	-0.0702	c_9	-7.1023×10^7

4.4 Combined measurement uncertainty estimation

Assuming the uncertainty distribution is Gaussian and that the standard uncertainties are uncorrelated, the combined uncertainty, in radians, can be estimated as the root sum of squares given by

$$u_\theta = \sqrt{\frac{u_{hm}^2}{2r_m h_m - h_m^{\,2}} + \frac{h_m^{\,2} u_{rm}^2}{2r_m^{\,3} h_m - r_m^{\,2} h_m^{\,2}} + u_b^{\,2} + u_f^{\,2}} \quad . \tag{1.4}$$

To better illustrate the effective boundaries when using the proposed technique, a two dimensional study was conducted using Equation 1.5 and the various parameters given throughout this paper. Figure 11 shows the estimated measurement uncertainty as a function of contact angle and droplet radius. The grey scale region of the scale bar in this figure is limited to the area of interest (1.5° and below) so that any part of the uncertainty surface exhibiting a pure white coloration indicates a region for which there will unacceptable measurement uncertainties by this criteria.

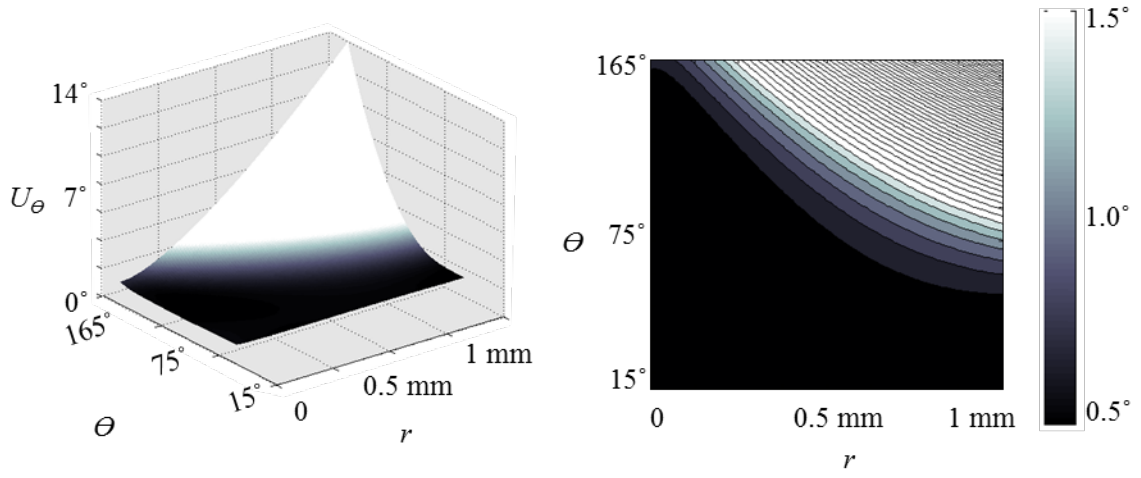

Figure 11: Plot of estimated measurement uncertainty for wetting contact angle measurement of water sessile drops when using a Keyence laser scanning confocal microscope.

4.5 Uncertainty example

To illustrate the use of these bi-cubic coefficients and other uncertainty components for derivation of combined uncertainties, consider the measurement of a water drop with a diameter of 1 mm resting on a

PTFE substrate in a normal air environment (contact angle assumed to be 110˚) using the Keyence confocal microscope and the measurement process outlined above. From the given geometric parameters, it is possible to calculate the values shown in Table 7 from which a combined measurement uncertainty of 0.9° is estimated.

Table 7: Values calculated/assumed in the estimation of uncertainty in aerial contact angle measurement of a 1 mm diameter water drop resting on a PTFE substrate when using a Keyence laser scanning confocal microscope.

Symbol	Description	Value
r_m	Measured radius (theoretical)	500 μm
h_m	Measured height (theoretical)	671 μm
u_{rm}	Uncertainty in measured radius	0.67 μm
u_{hm}	Uncertainty in measured height	0.76 μm
u_b	Uncertainty due to machine bias	0.36° [0.0062 rad]
u_f	Uncertainty due to spherical approximation	0.832° [0.0145 rad]
$u_{rm}^2\left(\frac{\delta\theta_c}{\delta r_m}\right)^2$	Contribution from radial measurement	0.00021° [3.66×10^{-6} rad]
$u_{hm}^2\left(\frac{\delta\theta_c}{\delta h_m}\right)^2$	Contribution from height measurement	0.00005° [8.61×10^{-7} rad]
u_θ	Combined measurement uncertainty	0.91° [0.0158 rad]

5 Conclusions

This paper has demonstrated a novel confocal measurement method to determine the geometry of sessile droplets. For spherical droplets on a flat surface, such a measurement can be used to determine the contact angle for wettability studies. The major advantage of this technique over traditional goniometry is

that the droplet can be measured from above, thereby eliminating the complexities in identifying triple phase contact line when viewing from an oblique angle. This aerial measurement is often more convenient for industrial quality control, particularly if viewing at an oblique angle is obscured. A further advantage of this method is that it can be used to determine the volumetric and other geometric features of the droplet with only calibration of displacement in a vertical axis being necessary, for which there are mature technologies providing nanometer uncertainty over ranges extending to tens of millimeters.

For droplets having diameters less than 1 mm and contact angles between 15° and 160°, these droplets approach spherical shape and their contact angles can be computed analytically with less than 1 % error. For larger droplets, gravitational deformation needs to be considered.

Four experimental studies have been carried out to assess the performance of this technique:

1. A direct comparison is presented of contact angle measurement on 5 µl glycerin droplets using both traditional goniometry, and the confocal technique, which resulted in a measured difference of 3.1° in the worst case.
2. A three technique comparison (goniometric, confocal and contact measurement), using stainless steel reference artifacts having nominal radius of 254 μm and apparent contact angles ranging from 45° to 113°, showed results differing by 7.9° across all three measurement techniques, and 0.87° between the confocal and contact methods.
3. A radius measurement repeatability experiment conducted on 254 μm radius spheres using a laser scanning confocal microscope yielded a mean radius of 255.6 μm with a standard deviation of 1.98 μm across the seven measurements.
4. Finally, a proof-of-concept study demonstrating the capability to confocally measure a 25.0 μm radius using the cat's eye method on a 50.0 μm diameter transparent glass sphere. The diameter of the sphere was measured as the height from the top surface to a plane fitted to the substrate on which it was placed. The height resolution in this experiment was 0.1 μm.

Generally, it has been found that contact angles can be repeatedly measured using this technique with deviations typically being less than 0.25° and often less than 0.1°. This level of repeatability is an improvement over the repeatability of droplet measurements using goniometric methods available in our laboratory that show deviations of 7° or more.

One issue that is currently unresolved is a lack of sub-millimetre reference spheres with known uncertainties that are traceable to standards. For larger spheres, this is being addressed by determination of mass using the crystal density methods for which uncertainties of a few nanometres have been achieved [24]. The radius of the steel spheres was measured using three methods, fitting from the surface map, the cats-eye and confocal distance, and using a surface plate and dial gauge. While these had a nominal radius of 0.254 mm, the three measured values were 0.2556 mm (number of measurements $n = 7$), 0.2576 mm ($n = 7$), and 0.2548 mm ($n = 14$) with deviations of 1.98 μm, 0.67 μm, and 0.63 μm respectively. Contact deformations cannot be ruled out for the smaller radius measured using the dial gauge. A student's 't' test comparing mean values between the cats-eye method and contact produces a value of $t = 9.4$, indicating a significant difference between these two measurements. A t value of 2.5 for the two optical measurements is inconclusive indicating a difference at the 5 % significance level and no difference at 2 %. While these deviations do not significantly impact the results in this paper, the absolute measurement of small spheres remains a metrology challenge.

While this study has measured droplets having diameters between 25 μm and 1 mm, in principle our method can be extended to other sizes. At lower bound, it is expected that this method is limited by the point-spread function of the confocal instruments, which is on the order of a few wavelengths. On the other hand, larger droplet size can also be measured by this method, provided that gravitational deformation can be accounted for. The simplicity of this method makes fast measurements practical, which could be applied to study droplet deposition processes, for example, contact angle hysteresis and contact angle variation over time.

Acknowledgements

This research was jointly funded by the Intel Corporation, by the Affiliates Program of the Center for Precision Metrology Affiliates Program, and by the UK National Measurement System Engineering & Flow Metrology Programme. Thanks to Gaurav Singh for help with laboratory measurements.

References

[1] Mack G L, Lee D A 1936 The determination of contact angles from measurements of the dimensions of small bubbles and drops. II. The sessile drop method for obtuse angles *J. Phys. Chem.* **40** 169–176

[2] Mittal K L 2008 *Contact angle, wettability and adhesion, vol 5* (CRC Press)

[3] Johnson R, Dettre R 1993 *Wetting of low-energy surfaces, vol 49* (Marcel Dekker: New York)

[4] ASTM D7334–08 2008 Surface wettability of coatings, substrates and pigments by advancing contact angle measurement

[5] Chesna J W, Rivers R I, Smith D T, Her T-H, Samara A M 2012 Reducing uncertainty of wettability measurements through controlled sessile droplet deposition: current issues *Proc. ASPE, San Diego, CA* 472-475

[6] Marmur A 2009 A guide to the equilibrium contact angles maze *Contact Angle, Wettability and Adhesion* **6** 3-18

[7] Obrien S B G M, van den Brule B H A A 1991 Shape of a small sessile drop and the determination of contact angle *J. Chem. Soc., Faraday Trans.* **87** 1579-1583

[8] Chesna J W, Her T-H, Smith S T 2014 Methods of determining the shape of a sessile drop US patent 0123785 A1

[9] Minsky M 1961 *Microscopy apparatus* US Patent 3,013,467.

[10] Artigas R 2011 *Imaging confocal microscopy*. In: Leach R K *Optical measurement of surface topography* (Spinger: Berlin).

[11] Anthony G T, Anthony H M, Cox M G, Forbes A B 1991 *The parametrization of geometric form* Technical Report EUR 13517 EN (Commission of the European Communities, Luxembourg).

[12] Leach R K, Giusca C L, Haitjema H, Evans C, Jiang X 2015 Calibration and verification of areal surface texture measuring instruments *Ann. CIRP* **64** 797-813.

[13] Giusca C L, **Leach R K** 2013 Calibration of imaging confocal microscopes for areal surface texture measurement *Measurement Good Practice Guide No*. 128 (National Physical Laboratory).

[14] Zhou Y, Ghim Y S, Fard A, Davies A 2013 Application of the random ball test for calibrating slope-dependent errors in profilometry measurements *Appl. Opt.* **52** 5925-5931.

[15] Schmitz T L, Gardner N, Vaughn M, Medicus K, Davies A 2008 Improving optical bench radius measurements using stage error motion data *Appl. Opt.* **47** 6692-6700.

[16] Sun R, Qiu L, Yang J, Zhao W 2012 Laser differential confocal radius measurement system *Appl. Opt.* **51** 6275-6281.

[17] Selberg L A 1992 Radius measurement by interferometry *Opt. Eng.* **3** 1961-1966.

[18] Weise W, Zinin P, Wilson T, Briggs A, Boseck S 1996 Imaging of spheres with the confocal scanning optical microscope *Opt. Lett.* **21** 1800-1802.

[19] Aguilar J F, Lera M, Sheppard C J R 2000 Imaging of spheres and surface profiling by confocal microscopy *Appl. Opt.* **39** 4621-4628.

[20] Coupland J M, Mandal R, Polodhi K, Leach R K 2013 Coherence scanning interferometry: linear theory of surface measurement *Appl. Opt.* **52** 3662-3670.

[21] Mauch F, Lyda W, Gronle M, Osten W 2012 Improved signal model for confocal sensors for object depending artefacts *Opt. Express* **20** 19936-19945.

[22] Fujii A, Hayashi S, Fujii S, Yanagi K 2014 Analytical study on optically measured surface profiles of referential geometry using a finite-difference time-domain method *Surf. Topog.: Met. Prop.* **2** 014004.

[23] Stallinga S, Rieger B 2010 Accuracy of the Gaussian point spread function model in 2D localization microscopy *Opt Express.* **18** 24461-76.

[24] Bartl G, Krystek M, Nicolaus A, Giardini W 2010 Interferometric determination of the topographies of absolute sphere radii using the sphere interferometer of PTB *Meas. Sci. Technol.* **21** 115101.